Journal of Alloys and Compounds xxx (xxxx) xxx

Contents lists available at ScienceDirect

Journal of Alloys and Compounds

journal homepage: www.elsevier.com/locate/jalcom

Giant anisotropy of magnetic properties of hydrated iron fluoridotitanate single crystal

A.A. Dubrovskiy[a,*], Yu.V. Knyazev[a], D.A. Velikanov[a], A.M. Vorotynov[a], N.M. Laptash[c], Yu.V. Gerasimova[a,b]

[a] Kirensky Institute of Physics, Siberian Branch of RAS, 660036 Krasnoyarsk, Russia
[b] Institute of Engineering Physics and Radio Electronics, Siberian Federal University, 660079 Krasnoyarsk, Russia
[c] Institute of Chemistry, Far Eastern Branch of RAS, 690022 Vladivostok, Russia

ARTICLE INFO

Article history:
Received 21 July 2021
Received in revised form 28 October 2021
Accepted 9 November 2021
Available online xxxx

ABSTRACT

Study of the magnetic properties of the $FeTiF_6 \cdot 6\ H_2O$ single crystal has shown that this compound is a two-dimensional antiferromagnet with a N é el temperature of T_N = 8 K and its magnetic moment anisotropy attains 7000% at a temperature of T = 4.2 K. The Mössbauer spectroscopy data unambiguously indicate the paramagnetic state of iron cations in the temperature range of 4.2–300 K. However, a sharp change in the difference between the quadrupole doublet linewidths at 10 K has been observed, which is consistent with the temperature of magnetic ordering. It has been suggested that the long-range magnetic order is established in the crystal through the formation of the exchange coupling revealed by the electron spin resonance measurements on the oriented single crystals.

1. Introduction

The $FeTiF_6 \cdot 6\ H_2O$ (hydrated iron fluoridotitanate - HITF) compound belongs to the vast family $ABF_6 \cdot 6\ H_2O$ (A = Mg, Zn, Fe, Co, Ni, Mn, or Cd and B = Ti, Si, Ge, Sn, or Zr), which crystallizes in the rhombohedrally distorted CsCl structure. The alternating $[A(H_2O)_6]^{2+}$ and $[BF_6]_2$ octahedra are bound by the hydrogen bonds O – H ··· F. The compounds can be divided into two groups with different thermodynamic characteristics (the entropy change during the phase transitions and dT_0/dp signs) [1–15]. The group-1 compounds undergo the phase transition $R\bar{3}$ P21/c; for the group-2 compounds, the data on the symmetry of the high- and low-temperature phases are questionable. The recent X-ray diffraction analysis of the HITF single crystals showed that the crystal structure belongs mainly to sp. gr. $R\bar{3}$ at room temperature and turns to sp. gr. P21/c upon cooling [4]. However, along with the structure variations, the crystals of this family exhibit the anomalous behavior of the magnetic susceptibility [5–10]. The $FeSiF_6 \cdot 6\ H_2O$ crystal attracted attention of the Mössbauer spectroscopy [15–18] and electron spin resonance (ESR) spectroscopy [15,19,20] specialists. The available comprehensive data on the magnetic anisotropy of the $FeSiF_6 \cdot 6\ H_2O$ and $NiTiF_6 \cdot 6\ H_2O$ crystals reveal the antiferromagnetic (AFM) behavior in a field applied in the symmetry plane and the paramagnetic behavior in a field with the perpendicular direction, i.e., are two-dimensional (frustrated) antiferromagnets [5–10].

In turn, frustrated antiferromagnetism has attracted attention of researchers for many decades. This is due to the fact that this type of ordering is easily described using the Ising or Heisenberg models, which greatly facilitates the processing of the results [21,22]. The quantum phase transition between the N é el-type AFM state and the quantum paramagnetic ground state in the two- and three-dimensional bipartite Heisenberg models with the intradimer and interdimer bonds is also well-studied [23].

In addition, low-dimensional antiferromagnets are known for the emergent forms, including spin liquids, strongly correlated topological phases of the topological superconductivity type, exotic magnetism, magnon condensates, and quantum phase transitions [24–28]. It stands to mention the emergence of two-dimensional van der Waals magnets down to the atomic layer thickness, which gives grounds for further investigations of quantum magnetism and spintronics [29–31] and the experimental observation of long-range transport of magnons in a quasi-two-dimensional van der Waals antiferromagnet $MnPS_3$ [32]. It was found that, with a decrease in the 2D $MnPS_3$ thickness, the magnon diffusion length shortens [32]. In addition, Chang et al. [33], when studying the behavior of the two-dimensional $MnBi_2Te_4$ topological insulators, established a quantum phase transition from the axion insulator to the Chern insulator with

* Corresponding author.
E-mail address: andre-do@yandex.ru (A.A. Dubrovskiy).

https://doi.org/10.1016/j.jallcom.2021.162748
0925-8388/

zero longitudinal resistance and the quantum Hall resistance h/e^2, where h is the Planck's constant and e is the elementary charge, in a moderate magnetic field. This makes it possible to implement the axion electrodynamics in condensed systems.

In [34], it was shown also that the 2D invariant Dzyaloshinskii–Moriya interaction can ensure the unprecedented control of the AFM order using a weak magnetic field. This can allow the creation of AFM devices with the high efficiency provided by the lack of necessity for strong magnetic fields and by the higher efficiency of antiferromagnets as compared with ferromagnets.

The above-cited studies showed that frustrated magnets exhibit numerous unique properties. Most results have been obtained recently, within the last five years, which means that these systems still have been understudied despite their undoubted fundamental importance.

Starykh [35] reviewed the theoretical and experimental studies on trigonal frustrated antiferromagnets. The review focused on the recently discovered collinear spin density wave and spin nematic states, which are characterized by completely forbidden transverse spin excitations with $S_z = \pm 1$. The review covers the results of many works and it is noteworthy that the number of theoretical studies exceeds by far the number of experimental ones. This is most likely due to the fact that such properties are inherent of a limited number of materials.

Here, we report on the magnetic properties of the $FeTiF_6 \cdot 6\ H_2O$ single crystals investigated using static magnetometry, the Mössbauer effect, and electron spin resonance (ESR).

2. Experimental

The synthesis and composition of yellowish-green high-quality HITF crystals were described in [4,36]. The magnetization was measured with a vibrating sample magnetometer [37] and a Quantum Design PPMS9T Physical Property Measurement System. The sample parameters are: mass is about ≈30 mg, length is ≈5.5 mm and width is ≈3.5 mm. The crystal placed in a cylindrical chamber in such a way that the sample was tightly clamped and could not turn in a magnetic field. The magnetic field was applied along the c axis (Fig. 1), when we are talking about the parallelism of the magnetic field to the third-order axis and along the direction b (Fig. 1), when we are talking about the case $H \perp c$. To check the correctness of the measurements, the same sample was examined on a device Quantum Design PPMS 9 T Physical Property Measurement System with the standard VSM supplied with this instrument. It should be noted that the magnetization curves obtained with two different devices were found to be fully identical. In Fig. 2 the data obtained on the first installation were shown, in Fig. 3 - the data obtained on the PPMS.

The Mössbauer spectra of the grinded single crystal were recorded at the Research Institute of Physics (Southern Federal University, Rostov-on-Don, Russia) on an MS-1104Em spectrometer in the transmission geometry with a Co^{57}(Rh) radioactive source in the temperature range of 4.2–300 K using a CFSG-311-MESS cryostat with a sample in the exchange gas based on a closed-cycle Gifford–McMahon cryocooler (Cryotrade Engineering). The spectra were processed by varying the entire set of hyperfine parameters using the linear least-squares method.

The ESR measurements were performed on a Bruker Elexsys E-580 spectrometer operating in the X range at room temperature on an oriented single crystal rotated relative to the crystallographic direction with a step of 10°. The external magnetic field modulation was 100 kHz and the field amplitude, 5 Oe. The first derivative of the absorption signal was recorded.

3. Results and Discussion

Fig. 2 shows the measured magnetization of the HITF single crystal as a function of the applied magnetic field (Fig. 2a) and temperature (Fig. 2b). The measurement conditions are given in the figure caption. Fig. 2c presents the Curie–Weiss law processing of the temperature dependence of the magnetization.

Upon temperature variation (Fig. 2b), the magnetization behaves differently in a magnetic field applied along different crystallographic directions: in an external magnetic field perpendicular to the third-order crystallographic axis, the magnetization decreases with increasing temperature, which corresponds to the paramagnetic behavior, while in the magnetic field directed along the third-order axis, the AFM behavior of the magnetization with a N é el temperature of $T_N \approx 8$ K is observed. It is noteworthy that the antiferromagnetic transition is stretched. This is typical of low-dimensional antiferromagnetism [38,39]. Another remarkble item is the magnetization anisotropy at the liquid helium boiling point ($T = 4.2$ K); the magnetization values in an external field of $H = 1$ kOe differ by almost two orders of magnitude, i.e., the anisotropy attains 7000%.

Fig. 2c presents temperature dependences of the reverse magnetization approximated by the Curie–Weiss law. At the paramagnetic behavior of the magnetization, the straight drawn from the high-temperature region passes, as expected, to the point $T = 0$ K, while the AFM curve goes to the negative temperature region with the corresponding paramagnetic Curie temperature $\Theta \approx -27$ K.

According to the data obtained, the HITF crystal has a nontrivial magnetic structure. The crystal exhibits the AFM properties in an

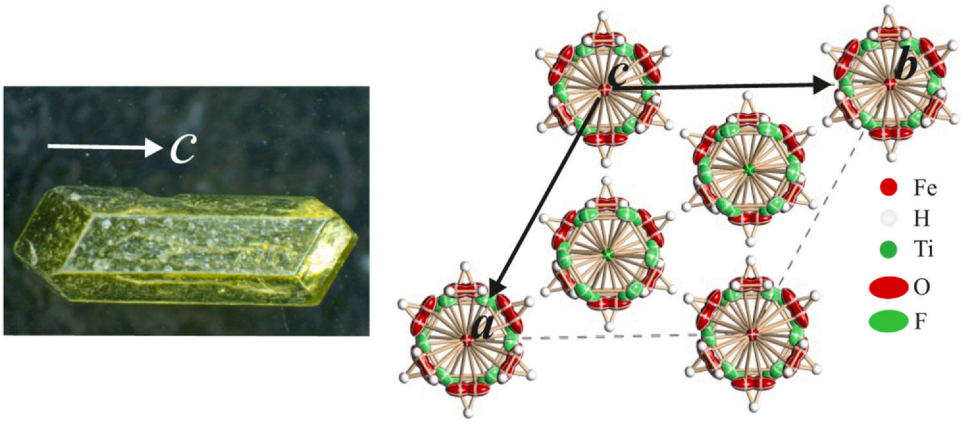

Fig. 1. HITF crystal with the c-axis direction (left) and crystal structure of this sample with the direction of symmetry axes.

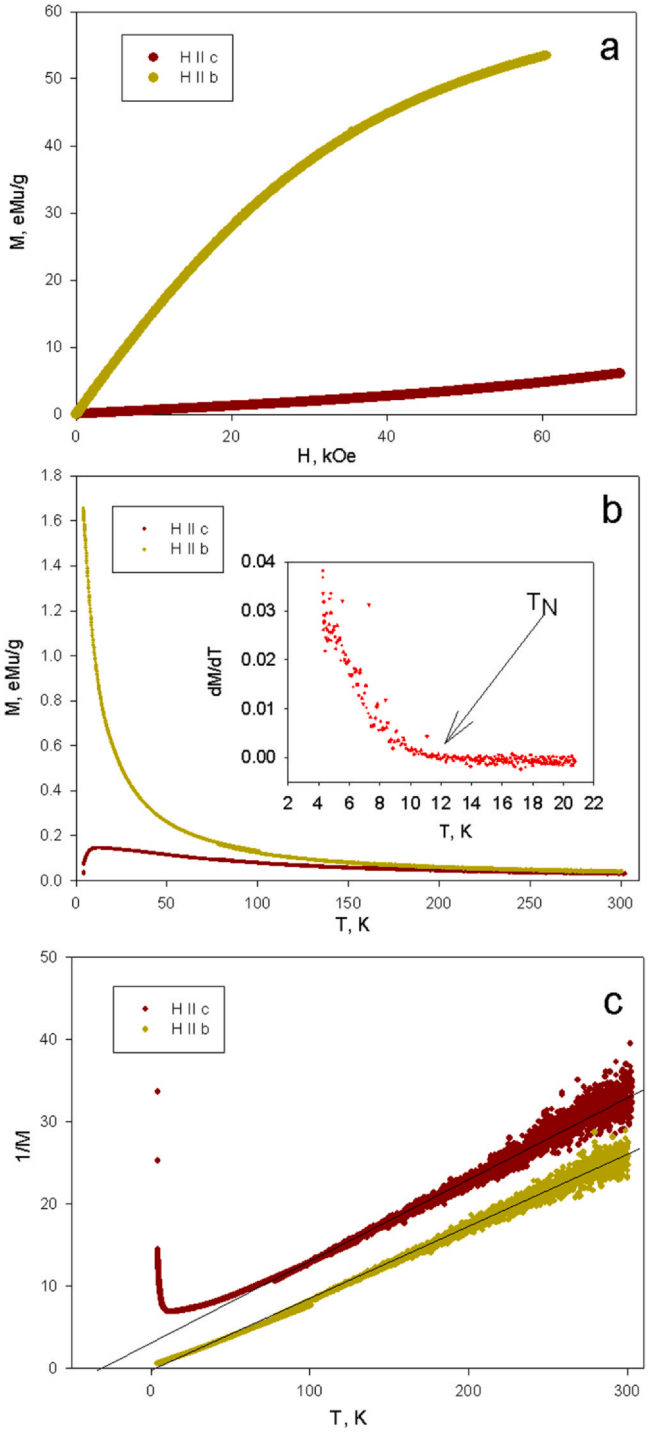

Fig. 2. (a) Magnetic field dependence of the magnetization at a measuring temperature of $T = 4.2$ K, (b) temperature dependence of the magnetization in a magnetic field of $H = 1$ kOe (inset: the derivative dM / dT, it changes sign at a temperature of about 11.8 K), and (c) Curie–Weiss law processing of the temperature dependences of the magnetization (green lines are an eye guide). The magnetic field directions relative to the crystal for all the plots are indicated by different colors (H II *c* stays for the field applied along the third-order crystallographic axis and H $\perp$ *c*, for the field perpendicular to it).

external magnetic field directed along the third-order crystallographic axis and behaves like a paramagnet in a field perpendicular to it. Thus, the HITF crystal is a two-dimensional antiferromagnet.

Fig. 3 shows temperature dependences of the magnetization measured in different magnetic fields and in the zero-field cooling

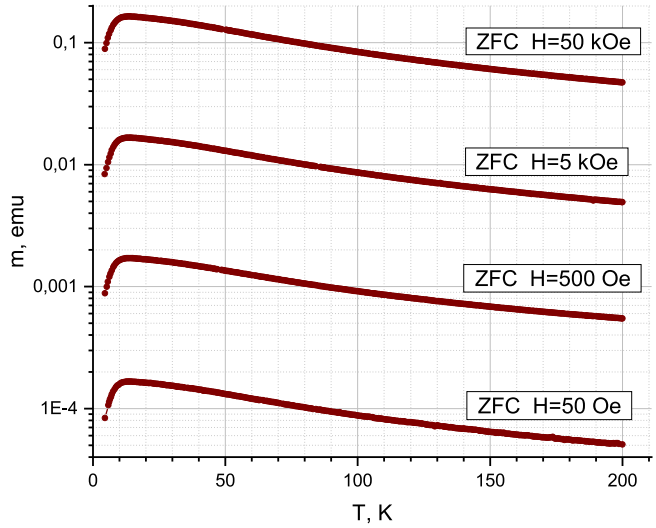

Fig. 3. Temperature dependences of the magnetization in different applied magnetic fields (shown in the figure). In all the measurements, the magnetic field is directed along the third-order crystallographic axis.

(ZFC) mode; the magnetic field direction in all the measurements coincided with the third-order crystallographic axis. It can be seen that, as the magnetization increases with the field, the maximum remains at a temperature of $T_N \approx 8$ K, which is also typical of an antiferromagnet.

3.1. Mössbauer Spectroscopy

Fig. 4 presents the Mössbauer spectra of the sample obtained at temperatures of 4.2 and 300 K. The shape of the spectra remains invariable in the range of 4.2–300 K and only temperature changes in the hyperfine parameters are observed (Table 1). The spectra are quadrupole doublets, the parameters of which are given in Table 1. Considering the obvious antiferromagnetic transition observed by magnetization measurements, we remarkably note that Mössbauer spectrum at 4.2. K of $FeTiF_6 \cdot 6\,H_2O$ does not show any feature of the Zeeman splitting (Fig. 4). It is evidence of the absence of the internal magnetic field on the ^{57}Fe nuclei in the zero-field Mössbauer experiment.

The results obtained are indicative of the charge state of the Fe^{2+} cations in the high-spin state in the H_2O octahedral environment [40,41]. The observed Fe^{3+} impurity doublet, which was previously mentioned in [42] for $FeSiF_6 \cdot 6\,H_2O$, can be attributed to the possible nonstoichiometry of the sample in the water molecule content. This nonstoichiometry can lead to the formation of the nonspecific-valence Ti^{3+} cations [36]. A fairly large width of this doublet also points out the inhomogeneity, which can be characteristic of defect states of the iron environment in a substance.

In [16,19,43], the spectra were simulated using two singlets, which allowed the authors to explain the structural transition in the $FeSiF_6 \cdot 6\,H_2O$ compound at $T = 230$ K observed in the form of a sharp change in the doublet linewidth difference. In our HITF measurements, the behavior of the difference $\delta W = W1 - W2$ between the widths of the right and left Lorentzian lines in the main doublet in the region of the observed magnetic transition was investigated (Fig. 4). The result is shown in Fig. 5. One can see a strong increase in the δW value around 10 K. The analogous δW growth in the region of the structural transition in $FeSiF_6 \cdot 6\,H_2O$ was attributed to the vibronic interactions induced by the dynamic Jahn–Teller effect [16,43]. These interactions lead to the anisotropy of nuclear vibrations in the sample. Under the action of the vibrational anisotropy caused by the Goldansky–Karyagin effect, the probability of the

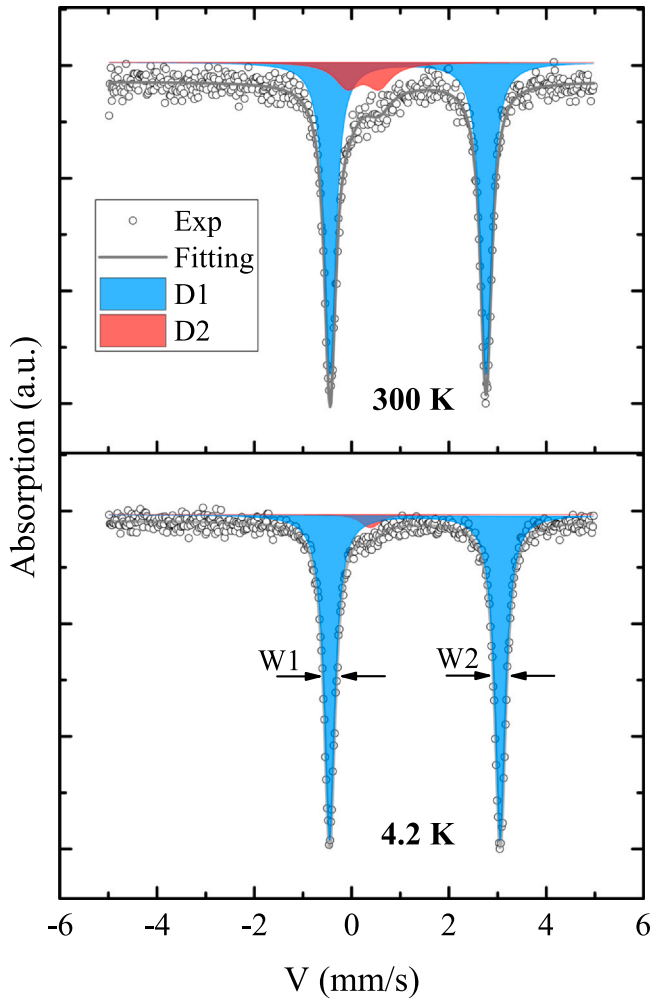

Fig. 4. Mössbauer spectra of the sample at temperatures of 4.2 and 300 K. Dots show the experimental spectra and the solid line, the results of processing. *W*1 and *W*2 are the full widths at half maximum for the main-doublet Mössbauer lines.

Mössbauer effect for iron nuclei in different crystallographic sites changes, which results in broadening of only one Mössbauer line.

Since the Mössbauer spectrum at $T = 4.2$ K has the form of a quadrupole doublet, we can unambiguously state that iron in the sample is in the paramagnetic state over the entire measuring temperature range. This is consistent with the results of numerous Mössbauer measurements performed on the $FeSiF_6 \cdot 6\,H_2O$ samples [16,44,45]. At the same time, the Mössbauer spectra of $FeSiF_6 \cdot 6\,H_2O$ in a magnetic field have a resolved hyperfine structure caused by the population of the electronic levels $S_z = \pm 2$ [16,19,43,44,46]. In order words, the Zeeman splitting can arise on the ^{57}Fe cores only under the action of an external field. Therefore, the existence of a long-range order in the crystal is not related to the superexchange coupling via oxygen or fluorine anions. Because the bonding of the metal-anion-metal is absent in this structure, the magnetic ordering should have a different origin. The observed giant anisotropy can play a key role in this process; for a more detailed study, the orientational measurements of the ESR spectra were performed.

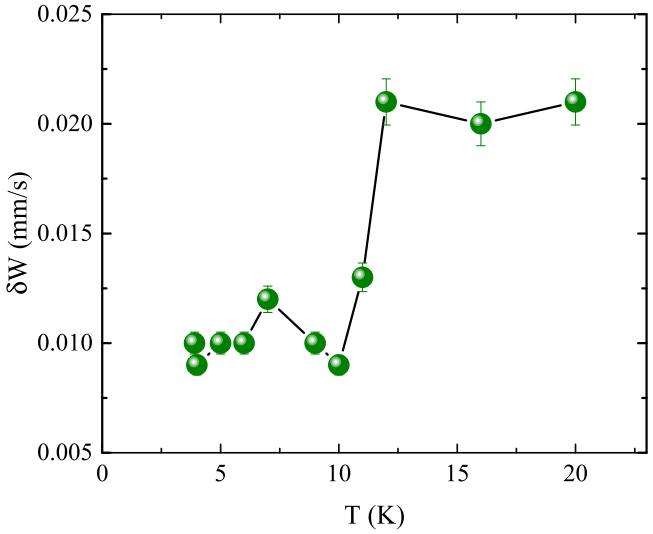

Fig. 5. Temperature variation in difference *D*1 between widths of the main-doublet Lorentzian lines near the magnetic transition in $FeTiF_6 \cdot 6\,H_2O$.

3.2. Electron Spin Resonance

The ESR spectra were measured on the HITF single crystal with the dilution of iron by the Mn^{2+} cations (0.02 mass %). Fig. 6 shows the ESR spectra for different orientations of the single crystal relative to the external magnetic field. Since the nuclear spin of the ^{56}Fe isotope has a value of $I = 0$, the ESR signal from the Mn^{2+} cations ($I = 5/2$) is only observed. In other words, the hyperfine structure highlighted in Fig. 6 as two regions to the left and to the right of the main intensity line is a manifestation of the hyperfine structure of manganese. Importantly, the Mn^{2+} cations, due to their symmetric electron shells (the orbital angular momentum is zero) does not contribute to the crystal anisotropy.

The spectra consist of the main line, which can be related to the ^{57}Fe isotope, and satellites of the Mn^{2+} hyperfine structure, the number of which is determined by the possible number of transitions in the form $(2I \pm 1)$. Therefore, six equidistant lines of the hyperfine structure are observed, which is consistent with the results that were obtained on iron fluoride silicates in [47]. The distance between these lines is ~100 Oe, according to the hyperfine structure constant of manganese ($A \sim 91–95 \cdot 10^{-4}$ cm^{-1}) [47,48]. The position of the main intensity line is independent of the single crystal orientation. At the same time, the positions and intensities of the satellites are highly sensitive to the orientation of the sample and determined by its anisotropy.

The computer simulation of the experimental spectra was performed in the approximation that the Mn^{2+} impurity ions occupy the iron sites in the oxygen environment. The simulation was performed with the spin Hamiltonian.

$$H = g_{iso}\mu_B SH + DS_z^2 + E(S_x^2 - S_y^2) + A_{iso}SI \quad (1)$$

Table 1
Mössbauer parameters of the $FeTiF_6 \cdot 6\,H_2O$ compound measured at room temperature. IS is the isomer chemical shift relative to α-Fe, QS is the quadrupole splitting, *W* is the absorption line width, and *A* is the site occupancy.

T, K	IS, mm/s ± 0.05	QS, mm/s ± 0.05	*W*, mm/s ± 0.05	*A*, % ± 0.03	Site
300 K	1.275	3.20	0.28	0.92	Fe^{2+}
	0.334	0.262	0.55	0.08	Fe^{3+}
4.2 K	1.434	3.55	0.29	0.97	Fe^{1+}
	0.500	0.146	0.40	0.03	Fe^{3+}

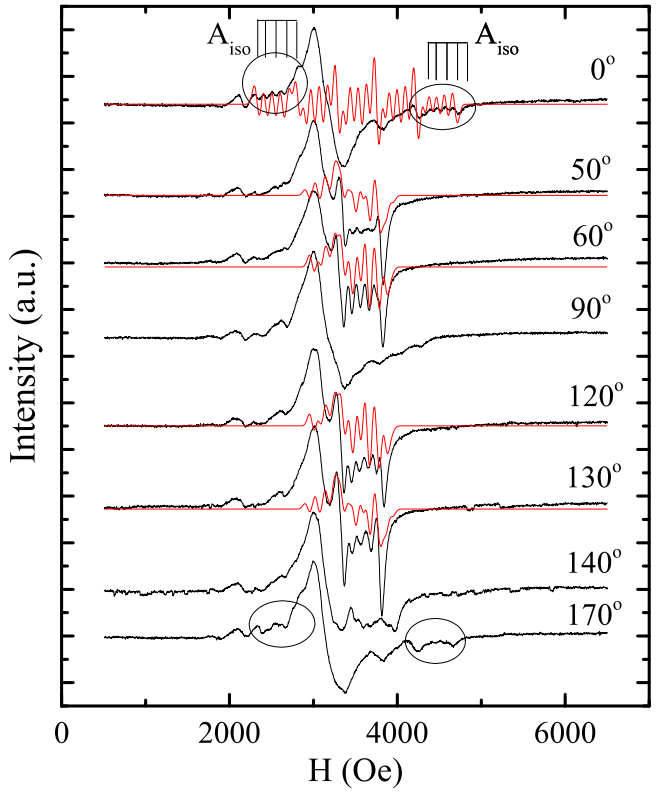

Fig. 6. ESR spectra at different orientations of the $FeTiF_6 \cdot 6\,H_2O$ single crystal relative to the applied field direction. The highlighted areas belong to the super-hyperfine structure of Mn. Red lines show the simulated spectra.

Table 2
ESR parameters of the spin Hamiltonian.

g_{iso}	$\|D\|$, Oe	E/D	A_{iso}, Oe
2	234	-0.16	95

where D and E are the spin Hamiltonian constants, g_{iso} is the g factor value, μ_B is the Bohr magneton, A is the isotropic constant of the hyperfine structure (HFS), and S and I are the electron and nuclear spins of the manganese ion. The obtained Hamiltonian constants are given in Table 2.

Upon rotation of the sample, we can observe a strong dependence of both the intensity of the super-hyperfine structure (SHFS) lines of the Mn^{2+} cations and their sites relative to the resonance line of the main intensity. The observed picture (Fig. 7) has some features. The SHFS lines have the highest intensity at angles of $\Theta = 60°$ and 120°; here, these lines are best resolved. This is explained by the crystal structure of the sample, which has a trigonal symmetry axis. The applied magnetic field is stronger than the dipole and hyperfine fields by an order of magnitude; i.e., the splitting is only observed in the field direction. The angular dependence of the hyperfine field is well-described by the equation $H_{res} \sim (3\cos^2\Theta - 1)$, where H_{res} is the resonance field and Θ is the angle between the field direction and the crystal trigonal axis. Such a dependence is typical of the uniaxial anisotropy [49].

It can be seen that the maximum resonance field is obtained in the direction of the trigonal crystal axis, which is the magnetic anisotropy axis of $FeTiF_6 \cdot 6\,H_2O$. Thus, this axis is the easy magnetization axis in this crystal.

The spin Hamiltonian parameter D for embedded manganese ions in the $FeTiF_6 \cdot 6\,H_2O$ structure was determined from the orientational ESR measurement data and is consistent with earlier studies [47,50]. This parameter for iron was determined from the ESR data in strong fields at high temperatures for the $FeSiF_6 \cdot 6\,H_2O$ samples. It attains huge values of about $D = 12\ cm^{-1}$ [16,19,20]. The resulting spin Hamiltonian parameter D determines the anisotropy constant, which, for the uniaxial anisotropy, is

$$K_1 \approx \frac{3}{4}\frac{\gamma D^2}{kT} \qquad (2)$$

where $\gamma = 4/9$ for Fe^{2+} [51]. Then, in the region of the transition temperature, the anisotropy constant for iron will attain $16\ cm^{-1}$. Since the Fe^{2+} cations are characterized by both the strong

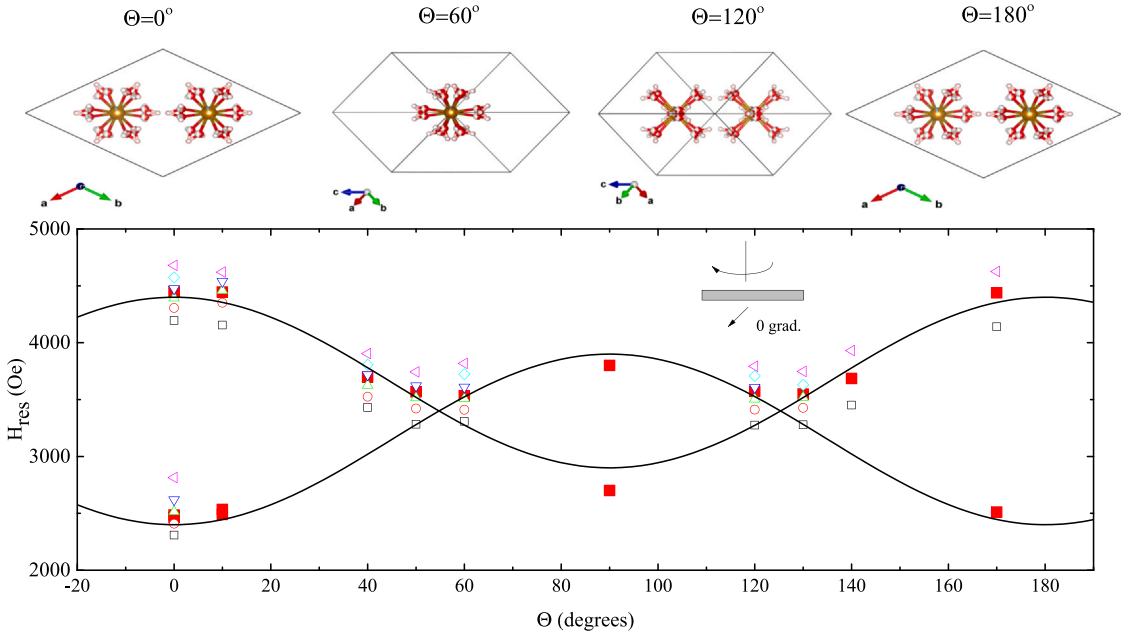

Fig. 7. Angular dependence of the resonance field obtained at 300 K upon rotation of the $FeTiF_6 \cdot 6\,H_2O$ crystal around its trigonal axis. Closed symbols show the position of the main line of the super-hyperfine structure of the ESR spectrum and open symbols, the relative positions of the lines of the super-hyperfine structure of the spectrum. The solid line shows the angular dependence $H_{res}(3\cos^2(\Theta) - 1)$.

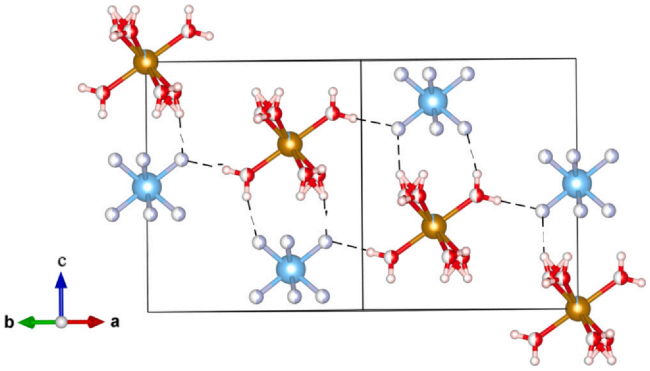

Fig. 8. $FeTiF_6 \cdot 6\,H_2O$ crystal structure. Dashed lines show hydrogen bonds.

spin–orbit coupling and the Jahn–Teller effect, the magnetic spin moment of iron will be directed along the easy (trigonal) crystal axis. This explains the giant magnetic anisotropy value discovered by us during the magnetic measurements.

4. Conclusions

To sum up, we can note the following. The magnetic properties of the $FeTiF_6{\cdot}6\,H_2O$ single crystal were investigated. This compound is a two-dimensional antiferromagnet with the Néel temperature $T_N = 8$ K, and its magnetic moment anisotropy reaches 7000% at a temperature of T = 4.2 K. The magnetization curve for the magnetic field directed along the third-order axis corresponds to the curve for the antiferromagnet. At the same time, in the magnetic field perpendicular to the third-order axis, the magnetization behaves paramagnetically.

As was previously noted for trigonal spinels with a low ordering temperature, the Jahn–Teller cations can have the magnetic moments directed only along their local trigonal axes, if the axial anisotropy energy is much higher than the exchange energy [52]. Then, it can be assumed that the strong anisotropy of the crystal and the possible exchange through hydrogen bonds (Fig. 8) [36,53] can explain the emergence of a long-range magnetic order below $T_N = 8$ K observed during the magnetic measurements.

CRediT authorship contribution statement

A.A. Dubrovskiy: Writing - Original Draft, Data Curation, Formal analysis, Funding, acquisition, Investigation, Visualization, Writing - Review & Editing. **Yu. V. Knyazev:** Investigation, Data Curation, Visualization, Writing - Original Draft, Methodology, Software, Writing - Review & Editing. **D. A. Velikanov:** Investigation, Software. **A.M. Vorotynov:** Investigation, Software. **N.M. Laptash:** Validation, Formal analysis, Investigation, Software. **Yu.V. Gerasimova:** Investigation, Visualization, Supervision, Writing - Review & Editing.

Declaration of Competing Interest

The authors declare that they have no known competing financial interests or personal relationships that could have appeared to influence the work reported in this paper.

Acknowledgements

The reported study was funded by Russian Foundation for Basic Research, Government of Krasnoyarsk Territory and Krasnoyarsk Regional Fund of Science according to the research project "Spectral and magnetic properties of single crystals of transition metal fluoride hexahydrates." No. 20–42-240014.

References

[1] I.N. Flerov, M.V. Gorev, S.V. Melnikova, M.L. Afanasyev, K.S. Aleksandrov, Study of phase transitions in $ABF_6{\cdot}6H_2O$ crystals, Fiz. Tverd. Tela 33 (1991) 1921–1929.
[2] I.N. Flerov, M.V. Gorev, K.S. Aleksandrov, M.L. Afanasyev, Effect of hydrostatic pressure on phase transitions in $ABF_6\ 6H_2O$ crystals (A identical to Zn, Co, Mg, Mn, Fe: B identical to Ti, Si), J. Phys.: Condens. Matter 4 (1) (1992) 91, https://doi.org/10.1088/0953-8984/4/1/020
[3] I.N. Flerov, M.V. Gorev, S.V. Melnikova, M.L. Afanasyev, K.S. Aleksandrov, Investigations of ferroelastic phase transitions in $ABF_6\ 6H_2O$ crystals (A: Zn, Co, Mg, Mn, Fe; B: Ti, Si), Ferroelectrics 143 (1) (1993) 11–16, https://doi.org/10.1080/00150199308008307
[4] A.A. Udovenko, E.A. Goreshnik, E.B. Merkulov, N.M. Laptash, Mixed-valence hydrated iron fluoridotitanate: Crystal structure and thermal behavior, J. Fluor. Chem. 249 (2021) 109853, https://doi.org/10.1016/j.jfluchem.2021.109853
[5] S.D. Roy, B. Ghosh, Phase transition studies of paramagnetic crystals at low temperatures, Pramana 28 (5) (1987) 573–581, https://doi.org/10.1007/BF03026694
[6] L.C. Jackson, The magnetic susceptibility of ferrous fluosilicate at low temperatures, Philos. Mag. 4 (38) (1959) 269–272, https://doi.org/10.1080/14786435908243263
[7] T. Ohtsuka, Crystalline Field Splitting in Ferrous Fluosilicate, -1245, J. Phys. Soc. Jpn. 14 (9) (1959) 1245, https://doi.org/10.1143/JPSJ.14.1245
[8] F. Varret, Pulsed magnetic field study of Fe^{2+} in some fluosilicates, J. Phys. Chem. Solids 37 (3) (1976) 257–263, https://doi.org/10.1016/0022-3697(76)90085-8
[9] F. Varret, Y. Allain, A. Miedan-Gros, Direct investigation of spin Hamiltonians DS2z by measuring magnetization during intense pulsed fields, Solid State Commun. 14 (1) (1974) 17–20, https://doi.org/10.1016/0038-1098(74)90222-1
[10] M. Karnezos, S.A. Friedberg, Magnetic and structural phase transitions in $NiTiF_6{\cdot}6H_2O$, J. Appl. Phys. 49 (3) (1978) 1380–1382, https://doi.org/10.1063/1.324998
[11] R.L. Davidovich, T.A. Kaidalova, T.F. Levchishina, X-ray diffraction data for some divalent metal fluorotitanates, J. Struct. Chem. 12 (1) (1971) 166–168, https://doi.org/10.1007/BF00744565
[12] R.S. Rubins, K. Kwee, Electron paramagnetic resonance of divalent nickel in the low temperature phases of magnesium fluosilicate and magnesium fluotitanate, J. Chem. Phys. 66 (9) (1977) 3948–3951, https://doi.org/10.1063/1.434445
[13] M.A. Heilbron, P.J. Gellings, Thermogravimetric investigations on $A(H_2O)_6BX_6$ complexes and the formation of ABX_6 and ABO_3 structures, Thermochim. Acta 17 (1) (1976) 97–105, https://doi.org/10.1016/0040-6031(76)80047-0
[14] A. Pastushenko, V. Lysenko, Electrochemical synthesis of luminescent ferrous fluorosilicate hexahydrate ($FeSiF_6{\cdot}6H_2O$) nano-powders, RSC Adv. 6 (10) (2016) 8093–8095, https://doi.org/10.1039/C5RA25183D
[15] J. Krzystek, D. Smirnov, C. Schlegel, J. Slageren, J. van, Telser, A. Ozarowski, High-frequency and -field EPR and FDMRS study of the $[Fe(H2O)_6]^{2+}$ ion in ferrous fluorosilicate, J. Magn. Reson. 213 (1) (2011) 158–165, https://doi.org/10.1016/j.jmr.2011.09.046
[16] D.C. Price, Static and dynamic crystal-field effects in ferrous fluosilicate, Can. J. Phys. 65 (10) (1987) 1280–1293, https://doi.org/10.1139/p87-203
[17] S.M. Skjaeveland, I. Svare, D.P. Tunstall, Proton spin-lattice relaxation in iron fluosilicate, Phys. Lett. A 47 (2) (1974) 121–122, https://doi.org/10.1016/0375-9601(74)90375-2
[18] T.P. Sinha, Influence of Electron-Phonon Coupling on the Mössbauer Quadrupole Interaction in $FeSiF_6{\cdot}6H_2O$, Phys. Status Solidi (b) 169 (2) (1992) 561–570, https://doi.org/10.1002/pssb.2221690227
[19] R.S. Rubins, H.R. Fetterman, Electron paramagnetic resonance in ferrous fluosilicate at submillimeter wavelengths, J. Chem. Phys. 71 (12) (1979) 5163, https://doi.org/10.1063/1.438290
[20] Z. Yi-Yang, Z. Min-Guang, Study of the structure of $FeSiF_6{\cdot}6H_2O$ by EPR and optical spectra, J. Phys. Chem. Solids 48 (8) (1987) 729–731, https://doi.org/10.1016/0022-3697(87)90067-9
[21] S. Dey, E.C. Andrade, M. Vojta, Destruction of long-range order in noncollinear two-dimensional antiferromagnets by random-bond disorder (R), Phys. Rev. BB 101 (2020) 020411, https://doi.org/10.1103/PhysRevB.101.020411
[22] N. Ma, P. Weinberg, H. Shao, W. Guo, D.X. Yao, A.W. Sandvik, Anomalous quantum-critical scaling corrections in two-dimensional antiferromagnets, Phys. Rev. Lett. 121 (2018) 117202, https://doi.org/10.1103/PhysRevLett.121.117202
[23] S. Sachdev, Quantum Phase Transition, Cambridge University Press, Cambridge, 2011, https://doi.org/10.1002/9780470022184.hmm108
[24] J.G. Rau, E.K.-H. Lee, H.-Y. Kee, Spin-Orbit Physics Giving Rise to Novel Phases in Correlated Systems: Iridates and Related Materials, Annu. Rev. Condens. Matter Phys. 7 (2016) 195–221, https://doi.org/10.1146/annurev-conmatphys-031115-011319
[25] D.N. Basov, R.D. Averitt, D. Hsieh, Towards properties on demand in quantum materials, Nat. Mater. 16 (2017) 1077, https://doi.org/10.1038/nmat5017
[26] B. Keimer, J.E. Moore, The physics of quantum materials, Nat. Phys. 13 (2017) 1045, https://doi.org/10.1038/nphys4302
[27] A. Bohrdt, F. Grusdt, M. Knap, Dynamical formation of a magnetic polaron in a two-dimensional quantum antiferromagnet, N. J. Phys. 22 (2020) 123023, https://doi.org/10.1088/1367-2630/abcfee
[28] T.J. Hicks, T. Keller, A.R. Wildes, Magnetic dipole splitting of magnon bands in a two dimensional antiferromagnet, J. Magn. Magn. Mater. 474 (2019) 512–516, https://doi.org/10.1016/j.jmmm.2018.10.136
[29] C. Gong, L. Li, Z. Li, H. Ji, A. Stern, Y. Xia, T. Cao, W. Bao, C. Wang, Y. Wang, Z.Q. Qiu, R.J. Cava, S.G. Louie, J. Xia, X. Zhang, Discovery of Intrinsic Ferromagnetism in Two-Dimensional van der Waals Crystals, Nature 546 (2017) 265, https://doi.org/10.1038/nature22060

[30] N. Samarth, Magnetism in Flatland, Nature 546 (2017) 216, https://doi.org/10.1038/546216a
[31] D.J. O'Hara, T. Zhu, A.H. Trout, A.S. Ahmed, Y. Luo, (Kelly), C.H. Lee, M.R. Brenner, S. Rajan, J.A. Gupta, D.W. McComb, R.K. Kawakami, Room Temperature Intrinsic Ferromagnetism in Epitaxial Manganese Selenide Films in the Monolayer Limit, Nano Lett. 18 (2018) 3125, https://doi.org/10.1021/acs.nanolett.8b00683
[32] Xing Wenyu, Qiu Luyi, Wang Xirui, Yao Yunyan, Ma Yang, Cai Ranran, Jia Shuang, X.C. Xie, Han Wei, Magnon transport in quasi-two-dimensional van der Waals antiferromagnets, Phys. Rev. X 9 (2019) 011026, https://doi.org/10.1103/PhysRevX.9.011026
[33] Liu Chang, Wang Yongchao, Li Hao, Wu Yang, Li Yaoxin, Li Jiaheng, He Ke, Xu Yong, Zhang Jinsong, Wang Yayu, Robust axion insulator and Chern insulator phases in a two-dimensional antiferromagnetic topological insulator, Nat. Mater. 19 (2020) 522–527, https://doi.org/10.1038/s41563-019-0573-3
[34] Hao Lin, D. Meyers, Suwa Hidemaro, Yang Junyi, Frederick Clayton, R.Dasa Tamene, Fabbris Gilberto, Horak Lukas, Kriegner Dominik, Choi Yongseong, Kim Jong-Woo, Haskel Daniel, J.Ryan Philip, Xu Haixuan, D.Batista Cristian, M.P.M. Dean, Liu Jian, Giant magnetic response of a two-dimensional antiferromagnet, Nat. Phys. 14 (2018) 806–810, https://doi.org/10.1038/s41567-018-0152-6
[35] Oleg A. Starykh, Unusual ordered phases of highly frustrated magnets: a review, Rep. Prog. Phys. 78 (5) (2015) 052502, https://doi.org/10.1088/0034-4885/78/5/052502
[36] S.V. Mel'nikova, N.M. Laptash, M.V. Gorev, E.I. Pogoreltsev, Mixed-valence hydrated iron fluoridotitanate: Synthesis, optics and calorimetry, J. Phys. Chem. Solids 142 (2020) 109444, https://doi.org/10.1016/j.jpcs.2020.109444
[37] A.D. Balaev, Y.V. Boyarshinov, M.M. Karpenko, B.P. Khrustalev, Automated magnetometer with superconducting solenoid, Instrum. Exp. Tech. (Engl. Transl.); (U. S.) 26 (3) (1985), ⟨https://www.osti.gov/biblio/5496232⟩.
[38] Jill C. Bonner, Fisher, E. Michael, Linear magnetic chains with anisotropic coupling, Phys. Rev. 135 (3A) (1964) A640, https://doi.org/10.1103/PhysRev.135.A640
[39] M. Baenitz, C. Geibel, M. Dischner, G. Sparn, F. Steglich, H.H. Otto, M. Meibohm, A.A. Gippius, $CuSiO_3$: A quasi-one-dimensional S=1/2 antiferromagnetic chain system, Phys. Rev. B 62 (18) (2000) 12201–12205, https://doi.org/10.1103/PhysRevB.62.12201
[40] P. Gütlich, E. Bill, A.X. Trautwein, Mössbauer spectroscopy and transition metal chemistry: fundamentals and applications, Springer Science & Business Media, 2010.
[41] Ho Spiering, R. Zimmermann, Go Ritter, Investigation of Hyperfine Interaction and Structure in FeSiF6·6HO2 by Mössbauer Measurements (doi.org/), Phys. Status Solidi (b) 62 (1) (1974) 123–133, https://doi.org/10.1002/pssb.2220620112
[42] F. Varret, J. Danon, Mössbauer investigation on the crystal field splitting of Fe2+ ion in zinc fluosilicate, Chem. Phys. Lett. 20 (6) (1973) 538–539, https://doi.org/10.1016/0009-2614(73)80493-2
[43] J. Chappert, G. Jehanno, F. Varret, Phase transformation and slow relaxation in fluosilicates: Mössbauer study, J. De. Phys. 38 (4) (1977) 411–418, https://doi.org/10.1051/jphys:01977003804041100/jpa-00208600
[44] C.E. Johnson, Hyperfine interactions in ferrous fluosilicate, Proc. Phys. Soc. (1958-1967) 92 (1967) 748, https://doi.org/10.1088/0370-1328/92/3/326
[45] A.J. Nozik, M. Kaplan, Significance of the Lattice Contribution to Mössbauer Quadrupole Splitting: Re-Evaluation of the Fe^{57} Nuclear Quadrupole Moment, Phys. Rev. 159 (2) (1967) 273, https://doi.org/10.1103/PhysRev.159.273
[46] H. Spiering, H. Vogel, W. Irler, The Phase Transformation in Ferreous Fluosilicate Hexahydrate, Phys. Status Solidi (b) 82 (1) (1977) 243–250, https://doi.org/10.1002/pssb.2220820126
[47] R.S. Rubins, J.E. Drumheller, S.L. Hutton, Electron paramagnetic resonance of Mn^{2+} in $FeSiF_6{\cdot}6H_2O$ and $FeSiF_6{\cdot}6D_2O$ above 100 K, J. Chem. Phys. 88 (1988) 92–94, https://doi.org/10.1002/pssb.2220820126
[48] R. Hrabański, EPR of Mn^{2+}-doped single crystals of $[Co(H_2O)_6]XY_6$ (X = Si, Sn, Pt; Y= F, Cl), Chem. Phys. Lett. 123 (3) (1986) 182–186, https://doi.org/10.1016/0009-2614(86)80009-4
[49] S. Krupička, Physik der Ferrite und der verwandten magnetischen Oxide. (Physics of Ferrites and related magnetic oxides) (in German) (Friedr.Vieweg + Sohn: Braunschweig), Springer-Verlag, 2013, https://doi.org/10.1007/978-3-322-83522-2
[50] R.S. Rubins, E.Drumheller John, Stuart L. Hutton, Phase transitions in $ZnTiF_6{\cdot}6H_2O$ observed by the electron paramagnetic resonance of Mn^{2+}, J. Chem. Phys. 91 (6) (1989) 3614–3617, https://doi.org/10.1063/1.456893
[51] R. Gerber, G. Elbinger, Contribution of Fe^{2+}, Mn^{3+} and Fe^{3+} ions to the magnetic anisotropy of $MgxMn_{0.6}Fe_{2.4-x}O_4$, J. Phys. C: Solid State Phys. 3 (6) (1970) 1363, https://doi.org/10.1088/0022-3719/3/6/019
[52] F. Varret, P. Imbert, Mössbauer study of Fe^{2+} ions in trigonal sites of spinels: $GeFe_2O_4$, $GeCo_2O_4$, $GeNi_2O_4$, J. Phys. Chem. Solids 35 (1974) 215–222, https://doi.org/10.1016/0022-3697(74)90037-7
[53] M. Bose, K. Roy, A. Ghoshray, H_2 NMR studies of structural phase transitions in some members of the deuterated $ABF_6{\cdot}6H_2O$ system, Phys. Rev. B 35 (1987) 6619, https://doi.org/10.1103/PhysRevB.35.6619